PRAMANA
— journal of
physics

Vol. 60, No. 1
January 2003
pp. 75–93

The phenomenon of nucleon emission at high angular momentum states of fused compound systems

T R RAJASEKARAN[1,*], S SELVARAJ[2] and S SANTHOSH KUMAR[3]
[1]Department of Physics, Manonmaniam Sundaranar University, Tirunelveli 627 012, India
[2]Department of Physics, The M.D.T. Hindu College, Tirunelveli 627 010, India
[3]Department of Physics, Madha Engineering College, Kunrathur 600 069, India
[*]Email: trrajasekaran@yahoo.com

MS received 2 July 2002; revised 31 August 2002

Abstract. Nucleon emission from high spin fused compound systems is analyzed in the framework of the statistical theory of hot rotating (STHR) nuclei. This is an elaborate version of our earlier work and we present our results for ^{156}Er, ^{166}Er, ^{168}Yb and ^{188}Hg. We predict an increase in neutron emission for ^{166}Er due to the abrupt decrease in neutron separation energy around $I \approx 55\hbar$. Since the drop in the separation energy is closely associated with the structural changes in the rotating nuclei, relative increase in neutron emission probability around certain values of angular momentum may be construed as evidence for the shape transition. A similar effect is predicted for ^{168}Yb around $I \approx 55\hbar$. We also extend the microscopic cranked Nilsson method (CNM) to hot nuclear systems and compare the results with that of the STHR method. The two methods yield different results for triaxially deformed nuclei although for biaxial deformations the results are identical. This is illustrated for ^{186}Hg.

Keywords. Separation energy; nucleon emission; shape transition; structural changes.

PACS Nos 21.10.Ma; 24.60.-k; 27.70.+q

1. Introduction

In [1], we have proposed a statistical approach to extract the nucleon separation energies for high spin hot nuclear systems, and demonstrated that the separation energy fluctuates with nuclear spin and that it is closely associated with the structural transitions of collective de-excitation of the system. This is contrary to the classical notion of monotonously decreasing separation energy with increasing angular momentum. We have reported in ref. [1] some results for ^{156}Er formed in the reaction ^{96}Zr (^{64}Ni,*xn*) ^{155}Er, which are in good agreement with the experimental results of Henss *et al* [2] for single neutron emission.

We present here an elaborate study of the neutron [3] and proton separation energies of high spin hot nuclei like ^{156}Er, ^{166}Er, ^{168}Yb and ^{188}Hg. Abrupt decrease in the neutron separation energies around $I \approx 55\hbar$ for ^{166}Er and ^{168}Yb is observed for excitation energies $E^* \approx 45$ MeV. It is conjectured that for these two nuclei, neutron emission probabilities

should increase sharply beyond $55\hbar$ for a given excitation energy. But as the angular momentum increases, a greater part of the excitation energy will be associated with the collective rotation rather than with the thermal heating which aids evaporation of nucleons. If one analyzes the neutron emission from hot high spin systems like ^{166}Er and ^{168}Yb around $30–60\hbar$, then it should be possible to observe an increase in emission probability around $55\hbar$ due to the abrupt fall in the neutron separation energy. In view of this phenomenon of enhanced neutron emission probability due to structural changes in the rotating system, we suggest that observance of relative increase in neutron emission around certain I values is an indication of structural transitions [4].

In the present work we also try to elaborate on the two methods of analyzing very high spin systems:

1. The statistical theory of hot rotating nuclei (STHR) developed by Moretto [5].
2. The cranked Nilsson oscillator model (CNM) extended to hot rotating nuclei in the present work.

In the STHR method of Moretto [5], the single particle levels of deformed nuclei are used and a Lagrangian multiplier projects out different angular momentum states of the system from the grand partition function [6]. The relationship between the Lagrangian multiplier γ and the collective frequency of rotation ω of the system have not been established hitherto, although it is obvious that they should be equal to one another as long as the single particle spin projections along the symmetry axis is a good quantum number. The single particle spin projections m_z is a good quantum number only for biaxial deformation of the system, i.e., axially symmetric shapes of the nuclei. However, for triaxial deformations the single particle spin projection m_z ceases to be a good quantum number since the matrix elements for a triaxially deformed system connects states of different m_z.

In the cranked Nilsson model (CNM) [7–9], the rotational part of the Hamiltonian $\vec{\omega}\cdot\vec{j}_z$, where ω is the rotational frequency, is diagonalized using oscillator basis [9]. The effect of $\vec{\omega}\cdot\vec{j}_z$ is to split states with spin projections $\pm m_z$, which are degenerate in the case of biaxial deformations. Since the Hamiltonian [10] for a triaxially deformed nuclei connects states of different m_z, the introduction of $\vec{\omega}\cdot\vec{j}_z$ gets contribution from all m_z states, and only $\langle j_z\rangle$ are known; $\langle j_z\rangle$ vanishes when the spins align in the direction perpendicular to the symmetry axis.

We have extended the cranked Nilsson model to hot nuclei and observe that the Lagrangian multiplier γ in the statistical model (STHR) [1,11–15] and rotational frequency ω in the CNM [8] are identical for the axially symmetric shapes and as triaxial deformation sets in, the values of ω and γ are different. This is illustrated for ^{186}Hg. We have also calculated other parameters of the nuclei like single particle level density parameter, neutron and proton separation energy, moment of inertia and the collective rotational energy of the system for spins ranging from 0 to $35\hbar$ and temperatures 0.3 and 1.0 MeV. Shape transitions are observed around spins $5\hbar$ and $20\hbar$ [15,16–19].

Pairing correlations are introduced along with the collective rotation and the interplay between various degrees of freedom like deformation, angular momentum, and temperature of the system and the pairing gap parameter Δ is an important aspect of the statistical method [1,5,13]. It is clear that the pairing correlations will inhibit states of higher angular momentum whereas rotation tries to break the pairs and align their spins along the direction of rotation. In §2, the cranked Nilsson Hamiltonian is described. We give a brief resume of the two methods (STHR and CNM) of studying high spin hot systems in §3 and §4. In §5,

methods of evaluating parameters like nucleon separation energies, level density parameter, moment of inertia and the collective rotational energy of the hot system are given. The results are presented and discussed in §6. Conclusion is drawn in §7.

2. Cranked Nilsson Hamiltonian

The Hamiltonian for the cranked Nilsson oscillator H^{ω} is given by [20]

$$H^{\omega} = H^0 - \vec{\omega}\cdot\vec{j_z}, \tag{2.1}$$

where H^0 is the triaxial Nilsson Hamiltonian which can be written as [10]

$$H^0 = p^2/(2m) + (m/2)(\omega_x^2 x^2 + \omega_y^2 y^2 + \omega_z^2 z^2) + c\vec{l'}\cdot\vec{s} + D(\vec{l'^2} - 2\langle\vec{l'^2}\rangle). \tag{2.2}$$

The three oscillator frequencies are given by

$$\omega_x = \omega_0 f_x(a_0, a_2) = \omega_0/[1 - a_0(16\Pi/5)^{-1/2} + a_2(8\Pi/15)^{-1/2}], \tag{2.3}$$

$$\omega_y = \omega_0 f_y(a_0, a_2) = \omega_0/[1 - a_0(16\Pi/5)^{-1/2} - a_2(8\Pi/15)^{-1/2}], \tag{2.4}$$

$$\omega_z = \omega_0 f_z(a_0, a_2) = \omega_0/[1 + a_0(4\Pi/5)^{-1/2}], \tag{2.5}$$

with the constraint that the total volume remains constant, i.e.,

$$\omega_x \omega_y \omega_z = \dot{\omega}_0^3, \tag{2.6}$$

where $\hbar\omega_0$ is the undeformed oscillator spacing given by

$$\hbar\omega_0 = 35\ \text{MeV}/(A^{1/3} + 0.77). \tag{2.7}$$

The deformation parameters a_0 and a_2 are varied in the range $a_0 = -0.6$ to $+0.6$ and $a_2 = 0.01$ to 0.06. For the Nilsson parameters κ and μ, values are chosen from ref. [21].

The triaxial Nilsson Hamiltonian is diagonalized in the cylindrical representation [9,10]. The non-rotational part of the Hamiltonian in eq. (2.1) can be written as

$$H^0 = \tfrac{1}{2}\hbar\omega_0[f_\rho\{-\nabla_\rho^2 + \rho^2\} + f_z\{-(\partial^2/\partial z^2) + z^2\}] + H' + C\vec{l'}\cdot\vec{s} + D(\vec{l'^2} - N(N+3)), \tag{2.8}$$

where

$$H' = \tfrac{1}{2}\hbar\omega_0 f_d\{-(\partial^2/\partial x^2) + (\partial^2/\partial y^2) + x^2 - y^2\}, \tag{2.9}$$

with

$$f_\rho = \tfrac{1}{2}(f_x + f_y) \text{ and } f_d = \tfrac{1}{2}(f_x - f_y). \tag{2.10}$$

The single particle spin projections m_z along the symmetry axis are also needed for the calculations. In eq. (2.1) the Hamiltonian reduces to the usual triaxially deformed nuclear Hamiltonian when ω is set to zero.

3. Statistical theory of hot rotating nuclei

We start with the grand canonical partition function for a system of N neutrons and Z protons in a state of total angular momentum M rotating about the symmetry axis z. The statistical properties of the system are contained in the grand partition function. The logarithm of the partition function for the superfluid nucleus Q_{BCS} is given by [5]

$$\ln Q_{BCS} = -\beta \sum_k (\varepsilon_k^n - \lambda_n - E_k^n) + \sum_k \ln\{1 + \exp[-\beta (E_k^n - \gamma m_k^n)]\} - \beta \Delta_n^2 / G_n, \tag{3.1}$$

where $E_k^n = [(\varepsilon_k^n - \lambda_n)^2 + \Delta_n^2]^{1/2}$ are the quasi-particle energies given in terms of single particle energies ε_k^n, chemical potential λ_n and the pairing gap Δ_n. The single particle levels ε_k^n correspond to the Hamiltonian given in eq. (2.1) with $\omega = 0$.

The average particle number, energy and angular momentum of the system are given by

$$\langle N \rangle = \sum_k 1 - \{(\varepsilon_k^n - \lambda_n)[\tanh \tfrac{1}{2}\beta (E_k^n - \gamma m_k^n)]/2E_k^n\} = \sum_k n_k^n, \tag{3.2}$$

$$\langle E_n \rangle = \sum_k \varepsilon_k^n \left[1 - \{(\varepsilon_k^n - \lambda_n)[\tanh \tfrac{1}{2}\beta (E_k^n - \gamma m_k^n)]/2E_k^n\}\right] - \Delta_n^2 / G_n, \tag{3.3}$$

$$\langle M_n \rangle = \sum_k [m_k^n / (1 + \exp \beta (E_k^n - \gamma m_k^n)]. \tag{3.4}$$

The pairing gap equation is given by

$$2/G_n = \sum_k [\tanh \tfrac{1}{2}\beta (E_k^n - \gamma m_k^n)]/2E_k^n, \tag{3.5}$$

where G_n is the pairing strength parameter [22]. The entropy S^n of the system is calculated using the equation

$$S^n = \sum_k \ln\{1 + \exp[-\beta (E_k^n - \gamma m_k^n)]\} + \beta \sum_k [(E_k^n - \gamma m_k^n)/(1 + \exp \beta (E_k^n - \gamma m_k^n))]. \tag{3.6}$$

The superscript n denotes neutrons. A similar set of equations exist for protons. The total angular momentum M, the total energy $E(M,T)$ and total entropy S are then obtained using

$$M = M_n + M_z, \tag{3.7}$$

$$E(M,T) = E_n(M,T) + E_z(M,T), \tag{3.8}$$

$$S = S^n + S^z. \tag{3.9}$$

As illustrated by Moretto [5], the laboratory-fixed z-axis can be made to coincide with the body-fixed z'-axis and it is possible to identify and substitute M for the total angular momentum I. In the quantum-mechanical limit, the z component M of the total angular momentum $M = M_n + M_z \rightarrow I + 1/2$ where I is the total angular momentum of the system.

The excitation energy $E^*(M,T)$ and free energy $F(M,T)$ of the system are given by

$$E^*(M,T) = E(M,T) - E_0, \tag{3.10}$$

$$F(M,T) = E(M,T) - TS. \tag{3.11}$$

where $E(M,T)$ is the total energy of the system for a given temperature T and E_0 is the ground state energy of the system.

It is important to note that the single particle levels ε_k^n correspond to the Hamiltonian given in eq. (2.1) with $\omega = 0$. This is the major difference between the two methods. Equations (3.2), (3.4) and (3.5) fix λ_n, γ and Δ_n in the pairing formalism. It should be noted here that when triaxial deformations are introduced, only average values of $m_z = \langle j_z \rangle$ contribute.

4. Cranked Nilsson oscillator model of hot rotating nuclei

Here we use the eigenvalues $\varepsilon_k(\omega)$ generated by cranked Nilsson Hamiltonian [7], given in eq. (2.1) with finite values of ω. The corresponding partition function is

$$\ln Q_{BCS}(\omega) = -\beta \sum_k (\varepsilon_k^n(\omega) - \lambda_k - E_k^n(\omega)) + \sum_k \ln[1 + \exp(-\beta E_k^n(\omega))] - \beta \Delta_n^2 / G_n \tag{4.1}$$

where $E_k^n(\omega) = [\,\varepsilon_k^n(\omega) - \lambda_n)^2 + \Delta_n^2]^{1/2}$ are the quasi-particle energies of the rotating system. The number, energy and angular momentum conservation equations for the superfluid state are

$$\langle N \rangle = \sum_k 1 - \{(\varepsilon_k^n - \lambda_n)[\tanh \tfrac{1}{2}\beta(E_k^n(\omega))]/2E_k^n(\omega)\} = \sum_k n_k^n, \tag{4.2}$$

$$\langle E_n \rangle = \sum_k \varepsilon_k^n \big[1 - \{(\varepsilon_k^n - \lambda_n)[\tanh \tfrac{1}{2}\beta(E_k^n(\omega))]/2E_k^n(\omega)\}\big] - \Delta_n^2/G_n, \tag{4.3}$$

$$\langle M_n \rangle = \sum_k [m_k^n/(1 + \exp\beta(E_k^n(\omega)))]. \tag{4.4}$$

The pairing gap equation is given by

$$2/G_n = \sum_k [\tanh \tfrac{1}{2}\beta(E_k^n(\omega)]/2E_k^n(\omega). \tag{4.5}$$

Here $m_k = \langle j_z \rangle$ are the average values of the operators j_z. The excitation energy of the system is given by

$$E_n^* = \sum_{k=1}^{\infty} \varepsilon_k^n(\omega) n_k^n - \sum_{k=1}^{N} \varepsilon_k^n(0). \tag{4.6}$$

The entropy S^n of the system is calculated using the equation

$$S^n = \sum_k \ln(1 + \exp[-\beta E_k^n(\omega)]) + \beta \sum_k E_k^n(\omega) / (1 + \exp[\beta E_k^n(\omega)]). \tag{4.7}$$

The superscript n denotes neutrons. A similar set of equations exist for protons. The total angular momentum M, the total energy $E(M,T)$ and total entropy S are then obtained using

$$M = M_n + M_z, \tag{4.8}$$

$$E(M,T) = E_n(M,T) + E_z(M,T), \tag{4.9}$$

$$S = S^n + S^z. \tag{4.10}$$

The excitation energy $E^*(M,T)$ and free energy $F(M,T)$ of the system are given by

$$E^*(M,T) = E(M,T) - E_0, \tag{4.11}$$

$$F(M,T) = E(M,T) - TS, \tag{4.12}$$

where $E(M,T)$ is the total energy of the system for a given temperature T and E_0 is the ground state energy of the system.

5. Methods of evaluating various parameters

5.1 *Nucleon separation energy*

As illustrated in ref. [1], we can extract the nucleon separation energy S_P and S_N using the free energy of the system. The general expression for neutron or proton separation energy would be

$$S_{N(P)} = \partial \Omega_N / \partial N, \tag{5.1}$$

where $\Omega_N = -T \ln Q$ and N is the number of neutrons or protons. In the STHR, '$\ln Q$' is defined by eq. (3.1) and in CNM '$\ln Q$' is defined by eq. (4.1). Substituting for Ω_N in the above equation we get

$$S_N = -T \frac{\partial \ln Q}{\partial \alpha_N} \frac{\partial \alpha_N}{\partial N}. \tag{5.2}$$

By definition,

$$\frac{\partial \ln Q}{\partial \alpha_N} = N.$$

In the absence of pairing correlations,

$$\frac{\partial \alpha_N}{\partial N} = \left[\sum_i [(1-n_i)n_i]\right]^{-1},$$

where n_i is the single particle occupation probability

$$n_i = \{1+\exp[\beta(\varepsilon_i + \gamma m_i - \mu)]\}^{-1}.$$

With pairing correlations the equation is written as

$$\frac{\partial \alpha}{\partial N} = \sum_i \frac{1}{2\beta E_k^n}\left[\left[\tanh\frac{1}{2}\beta(E_k^n - \gamma m_k^n)\right] + \frac{(\varepsilon_k^n - \lambda_n)^2}{E_k^2}\right]$$
$$\times\left\{\left[\sec h^2\frac{1}{2}\beta(E_k^n - \gamma m_k^n)\frac{\beta E_k^n}{2}\right] - \left[\tanh\frac{1}{2}\beta(E_k^n - \gamma m_k^n)\right]\right\}. \quad (5.3)$$

When $T \geq 0.5$ MeV as is usually the case in most of the fused compound systems, i.e., when the pairing correlations are not significant, the expression for the neutron (proton) separation energy is

$$S_{N(P)} = TN\left\{\sum_i [(1-n_i)n_i]\right\}^{-1}. \quad (5.4)$$

Results of the calculations are presented in figures 1a and 1b for the nuclei ^{156}Er, ^{166}Er, ^{168}Yb and ^{188}Hg without pairing and figures 1c and 1d with pairing. The values of S_P and S_N obtained using the two methods are discussed in §6.

5.2 *The single particle level density parameter*

The single particle level density parameter $a(M,T)$ as a function of angular momentum M and temperature T is extracted using the equation [13]

$$a(M,T) = S^2(M,T)/4E^*(M,T). \quad (5.5)$$

The results for the nuclei ^{156}Er, ^{166}Er, ^{168}Yb and ^{188}Hg are presented in figures 2a and 2b and are discussed in §6.

5.3 *Collective rotational energy*

Using eqs (3.3), (3.4), (4.3) and (4.4) we have calculated [1] the rotational energy E_{rot} at spin M as

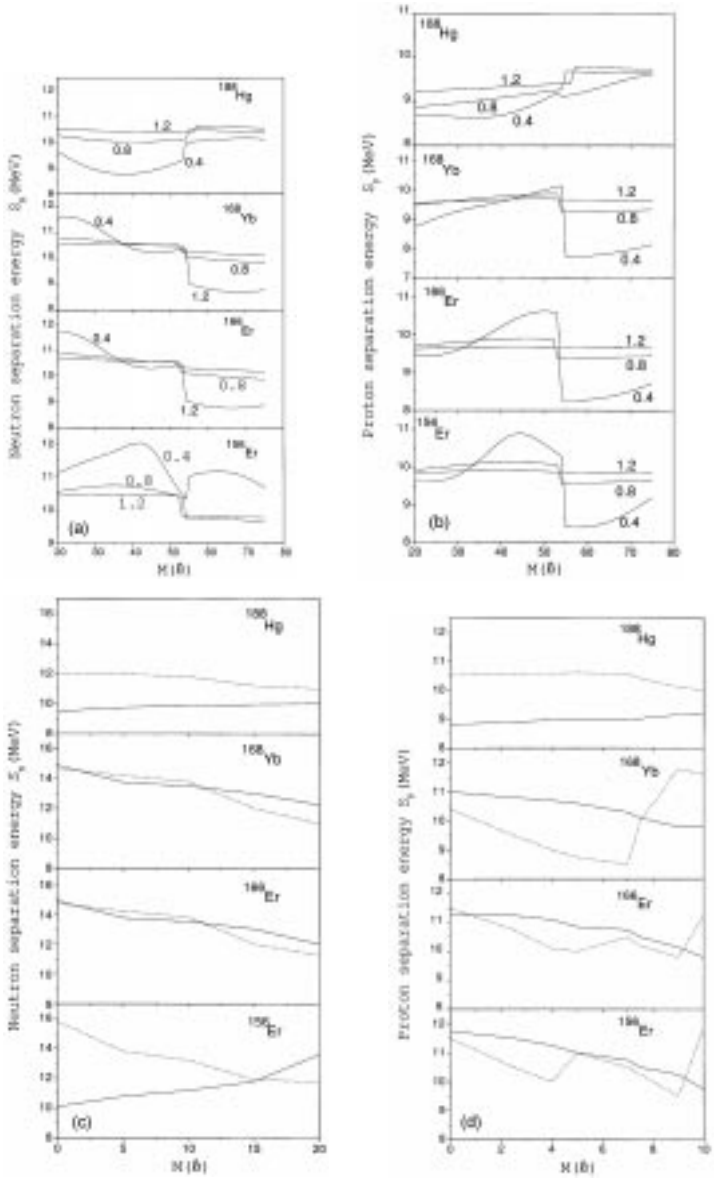

Figure 1. (**a**) The neutron separation energy S_N as a function of angular momentum M and T, without pairing correlations, for ^{156}Er, ^{166}Er, ^{168}Yb and ^{188}Hg. The numbers on the curve refer to the temperature T in MeV. (**b**) The proton separation energy S_P as a function of angular momentum M and temperature T, without pairing correlations for ^{156}Er, ^{166}Er, ^{168}Yb and ^{188}Hg. The numbers on the curve refer to the temperature T in MeV. (**c**) The neutron separation energy S_N with (dashed curve) and without (solid curve) pairing correlations for ^{156}Er, ^{166}Er, ^{168}Yb and ^{188}Hg with $T = 0.3$ MeV. (**d**) The proton separation energy S_P with (dashed curve) and without (solid curve) pairing correlations for ^{156}Er, ^{166}Er, ^{168}Yb and ^{188}Hg with $T = 0.3$ MeV.

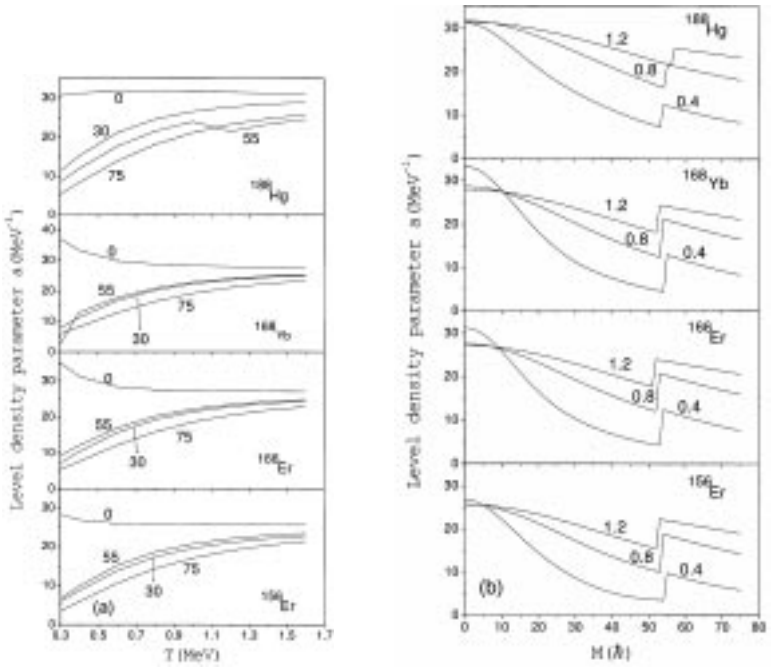

Figure 2. (**a**) The single particle level density parameter a as a function of T for various M for ^{156}Er, ^{166}Er, ^{168}Yb and ^{188}Hg. The numbers on the curve refer to the angular momentum M in units of $\hbar$. (**b**) The single particle level density parameter a as a function of M for various T for ^{156}Er, ^{166}Er, ^{168}Yb and ^{188}Hg. The numbers on the curve refer to the temperature in MeV.

$$E_{\rm rot} = E(M,T) - E(0,T). \tag{5.6}$$

The collective rotational energy has been used to calculate the nucleon emission probability. The result of the two methods is presented in figures 3a and 3b and is discussed in §6.

5.4 *Moment of inertia*

The moment of inertia is obtained using the expressions [8,23]

$$\theta_1 = \hbar^2 I(\partial E_{\rm rot}/\partial I)^{-1}, \tag{5.7}$$

$$\theta_2 = \hbar^2(\partial^2 E_{\rm rot}/\partial I^2)^{-1}. \tag{5.8}$$

The first expression is a global one whereas the second is a local definition of the moment of inertia. Note that when $E_{\rm rot} \propto I^2$ both the expressions yield the same result. These values of the moment of inertia are used in extracting neutron emission probability. The results are presented in figures 4a–4d.

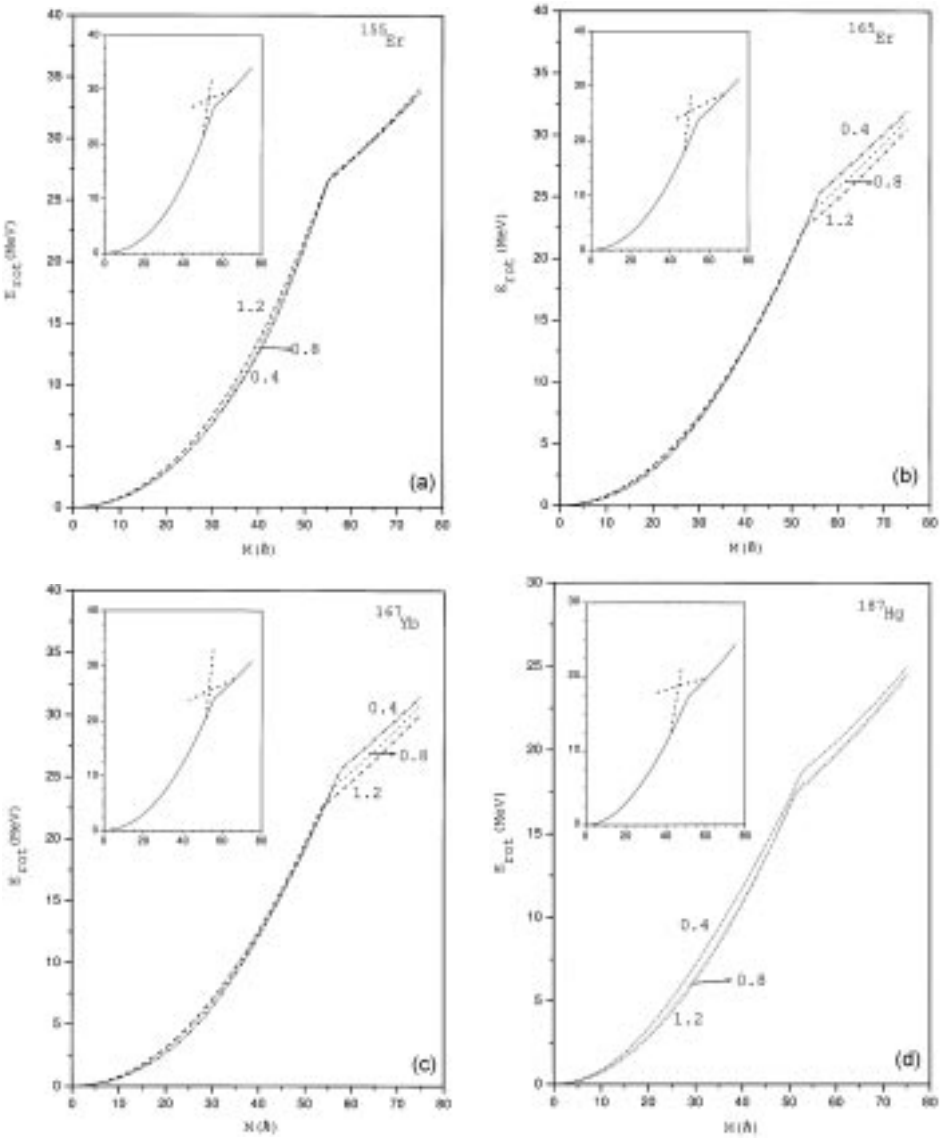

Figure 3. (**a**) The rotational energy as a function of angular momentum M and temperature T for ^{155}Er. The numbers on the curve refer to the temperature in MeV. The insert graph is for $T = 0.8$ MeV and the dotted line indicates the band crossing. (**b**) As in figure 3a for ^{165}Er. (**c**) As in figure 3a for ^{167}Yb. (**d**) As in figure 3a for ^{187}Hg.

5.5 *Nucleon emission probability*

The number of neutrons emitted within an energy interval E_n and $(E_n + \mathrm{d}E_n)$ is evaluated using [24]

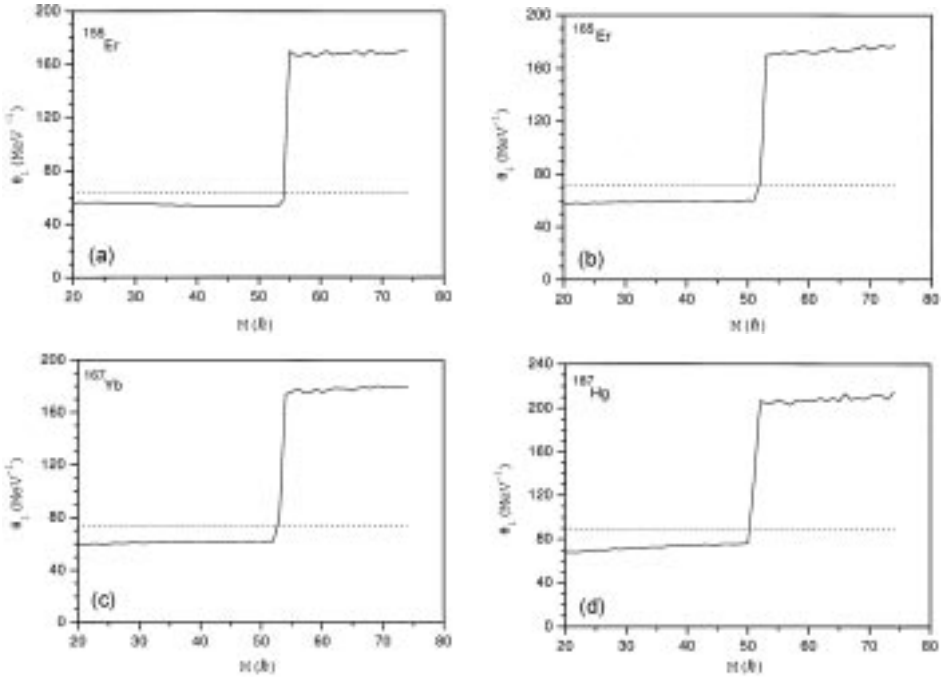

Figure 4. (**a**) Moment of inertia as a function of M for ^{155}Er. Solid line represents the moment of inertia calculated using eq. (5.9) and dotted line represents the moment of inertia of the rigid spherical nucleus. (**b**) As in figure 4a for ^{165}Er. (**c**) As in figure 4a for ^{167}Yb. (**d**) As in figure 4a for ^{187}Hg.

$$\phi(E_n) = \mathrm{d}N(E_n)/\mathrm{d}E_n = CE_n\,\rho(U), \tag{5.9}$$

where $U = E^* - E_{\mathrm{rot}} - S_N - E_n$ and E_n is the outgoing neutron energy, and the level density $\rho(U)$ at an excitation U is obtained using the formula [25]

$$\rho(U) = [\,\hbar^2/2\theta)^{3/2}(2I+1)\sqrt{a}\exp(2\sqrt{aU})]/[12(U+T)^2]. \tag{5.10}$$

In the above equation, θ is the moment of inertia and a is the single particle level density parameter. The neutron emission spectra are plotted in figures 5a–5d for various angular momentum.

5.6 *The relationship between γ and ω*

In the STHR method, eq. (3.4) is used to generate different angular momentum states for a given temperature and particle number. Calculations have been performed for ^{186}Hg for temperature 0.3 and 1.0 MeV. The values of the Langrangian multiplier γ is plotted vs. temperature and angular momentum. In the CNM method, eq. (4.4) is used to generate the different angular momentum states for the same nucleus ^{186}Hg and for the

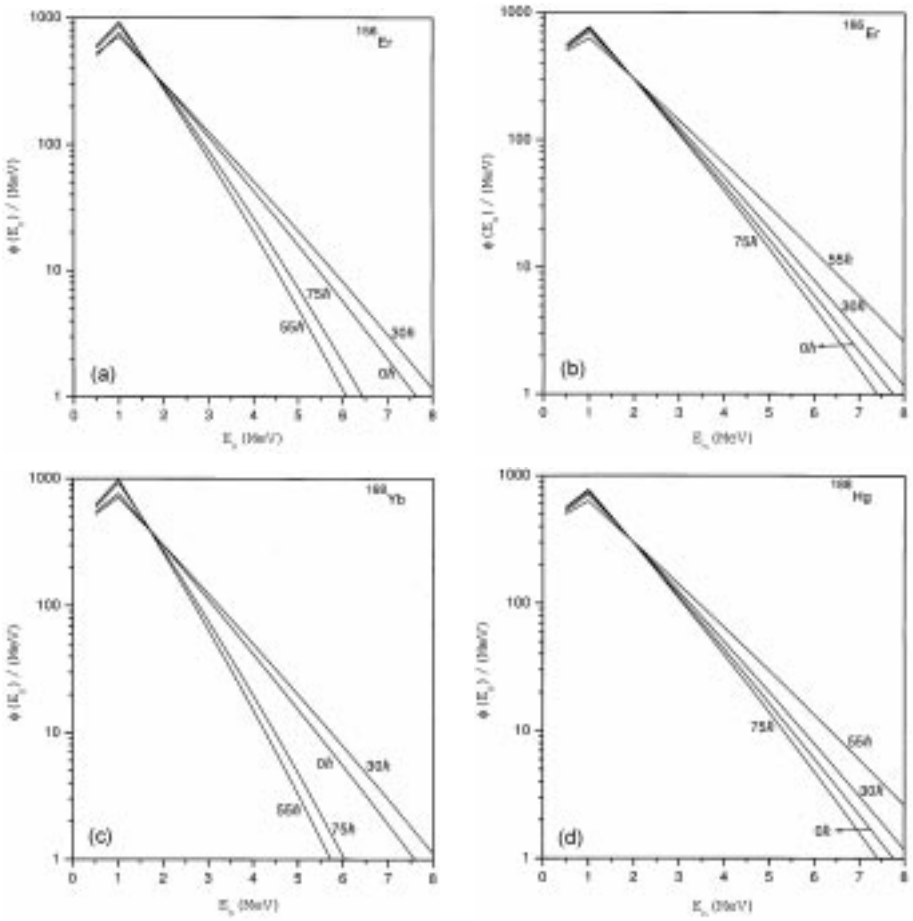

Figure 5. (**a**) Neutron emission spectrum for various spins for ^{156}Er. (**b**) As in figure 5a for ^{166}Er. (**c**) As in figure 5a for ^{168}Yb. (**d**) As in figure 5a for ^{188}Hg.

same temperature. The values of the rotational frequency ω are plotted vs. temperature and angular momentum. From figure 6a, it is obvious that $\gamma = \omega$ for biaxial deformation and $\gamma \neq \omega$ for triaxial deformations. Also for triaxially deformed nuclei the various parameters evaluated in the previous sections using the two methods yield different results. The result is shown in figures 6–12.

6. Results and discussions

Classically one expects the neutron separation energy to decrease with increasing angular momentum of the system. This may be true for systems with uniform distribution of matter rotating at constant speed. However, when the system is made of constituent elementary sub-systems with individual spins and momenta, the separation energy depends on the structural fluctuations associated with rotation of the microscopic system.

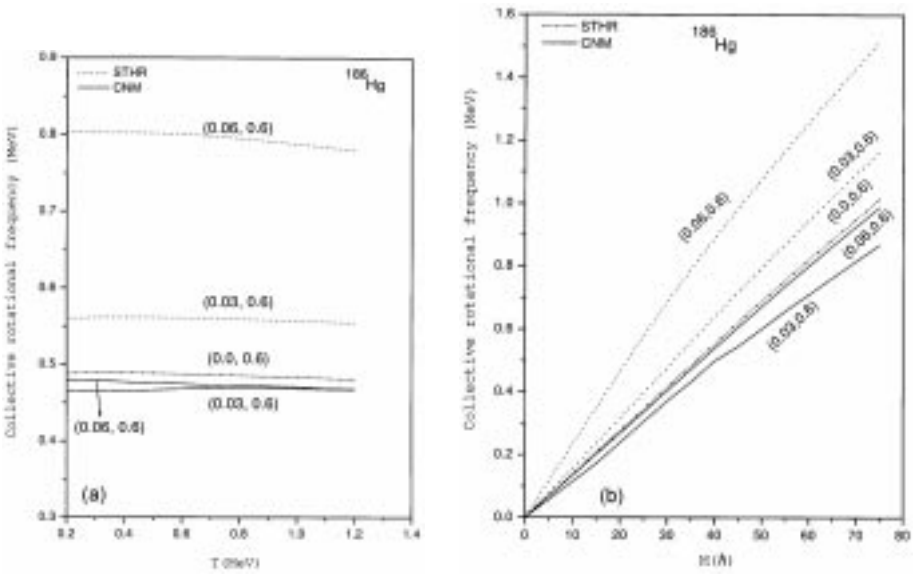

Figure 6. (**a**) Collective rotational frequency for ^{186}Hg as a function of temperature T and deformation for $M = 30\hbar$ using the STHR and CNM calculations. The deformation parameters a_2 and a_0 are shown in the figure, the first coordinate being a_2 and the second one being a_0. (**b**) Collective rotational frequency for ^{186}Hg as a function of angular momentum M and deformation for $T = 1.0$ MeV using the STHR and CNM calculations. The deformation parameters a_2 and a_0 are shown in the figure.

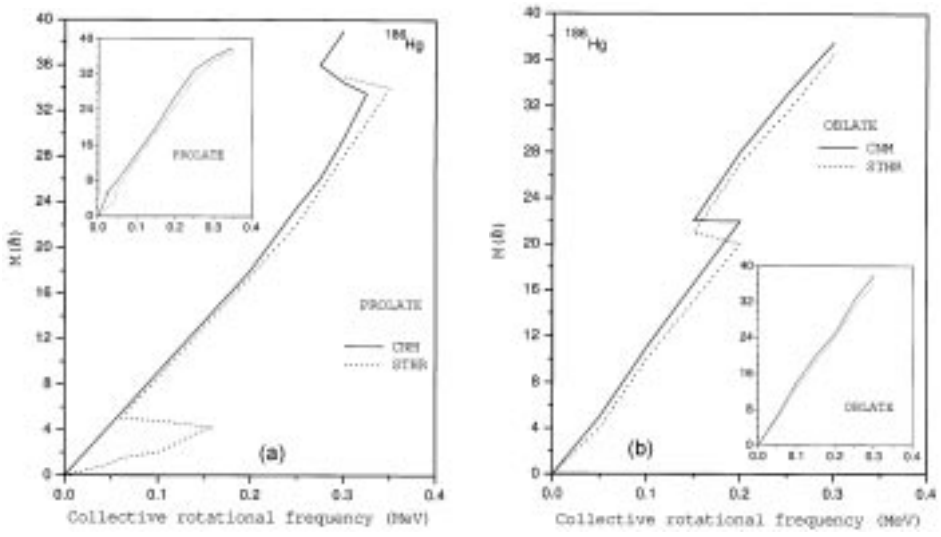

Figure 7. (**a**) Collective rotational frequency vs. M for $T = 0.3$ MeV, for prolate deformation. The insert graph is for $T = 1.0$ MeV. The axes of the inset graph are the same as the main graph. (**b**) As in figure 7a for oblate deformation.

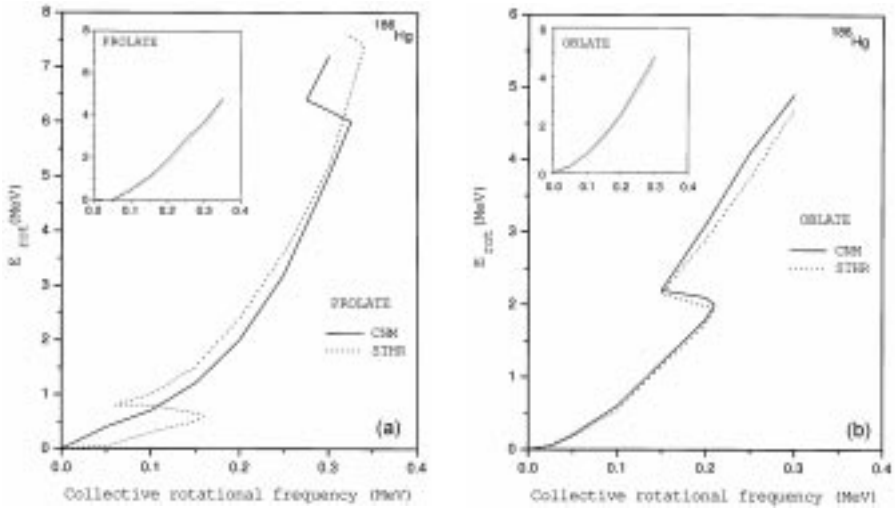

Figure 8. (**a**) Collective rotational frequency vs. collective rotational energy $E_{\rm rot}$, for $T = 0.3$ MeV, for prolate deformation. The insert graph is for $T = 1.0$ MeV. The axes of the insert graph are the same as the main graph. (**b**) As in figure 8a for oblate deformation.

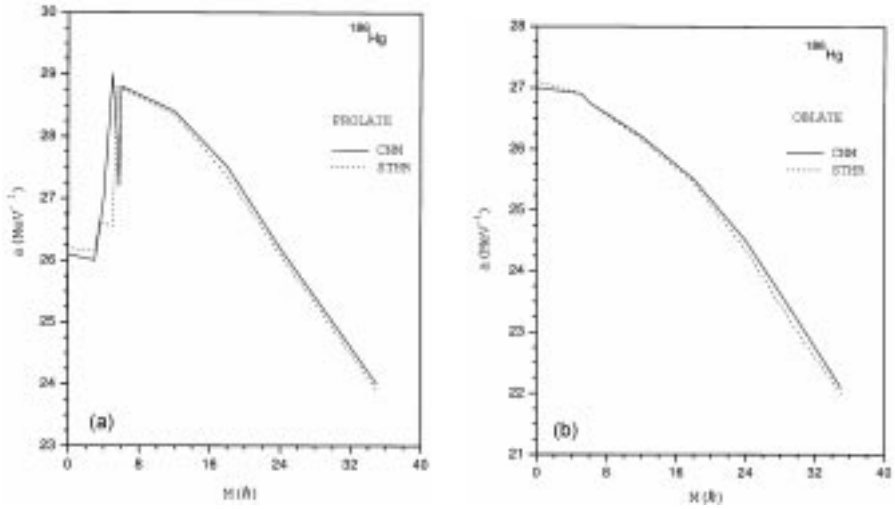

Figure 9. (**a**) The single particle level density parameter a as a function of angular momentum M for $T = 1.0$ MeV using STHR and CNM calculations, for prolate deformation. (**b**) As in figure 9a for oblate deformation.

Since the statistical theory employed in the present study takes into account the behavior of nucleons and their reactions to the collective rotation induced by the transfer of relative angular momentum and kinetic energy into intrinsic excitation of the system with several modes of de-excitation, it should be the appropriate formalism for application to the study of particle number and angular momentum fluctuations in hot rotating nuclei.

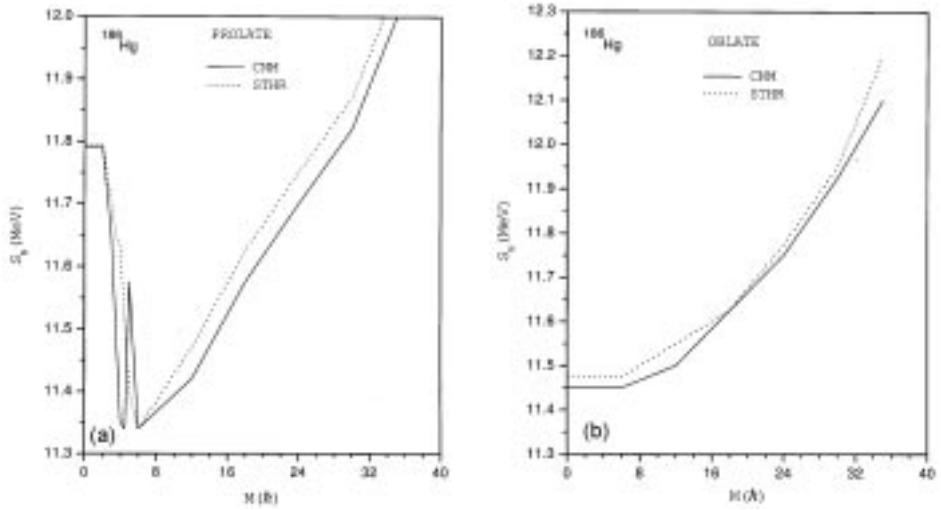

Figure 10. (**a**) Neutron separation energy S_N vs. angular momentum M for $T = 1.0$ Mev using STHR and CNM calculations, for prolate deformation. (**b**) As in figure 10a for oblate deformation.

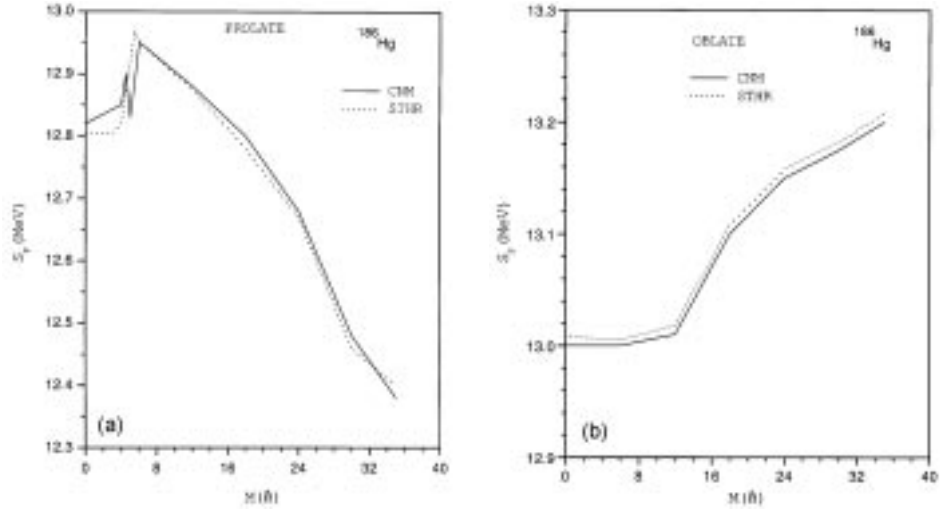

Figure 11. (**a**) Proton separation energy S_P vs. angular momentum M for $T = 1.0$ MeV, for prolate deformation. (**b**) As in figure 11a for oblate deformation.

The neutron separation energy S_N is shown as a function of spin up to $75\hbar$ in figure 1a for ^{156}Er, ^{166}Er, ^{168}Yb and ^{188}Hg without pairing correlations. There is a general tendency for these heavier high spin systems to experience an abrupt change in the neutron separation energy beyond $50\hbar$. This abrupt fall in S_N by about 0.5 to 1.5 MeV should result in an increase in neutron emission for high spins provided the system has enough excitation energy. For the cases considered above, the excitation energy E^* around temperature

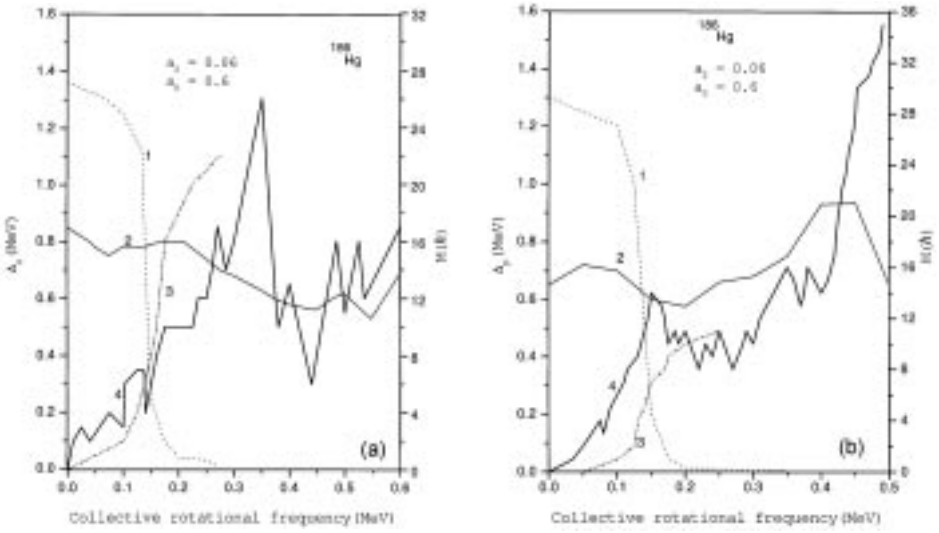

Figure 12. (**a**) Neutron gap parameter Δ_n as a function of collective rotational frequency for $T = 0.3$ MeV, for ^{186}Hg. The numbers 1 and 2 on the curve correspond to the Δ_n obtained by the STHR and CNM calculations respectively. The corresponding spins generated by the two methods are shown in curves 3 and 4. (**b**) As in figure 12a for proton gap parameter Δ_p.

1.2 MeV is roughly 35 to 45 MeV. The minimum value of S_N occurs at $I = 55\hbar$ for almost all nuclei, corresponding to shape transition from prolate to oblate [26,27]. This seems to be a feature of $N = 88$ systems, since similar structural changes has been reported by Cranmer-Gorden *et al* [28] for ^{154}Dy which is also an $N = 88$ system. Since $N = 88$ isotones lie between $N = 86$ isotones (which have a spherical ground state with rotational states built by nucleon alignments near Fermi energy), and $N = 90$ isotones (which have a prolate ground state configuration with high spins developed by collective rotation and nucleon alignments), they are subjected to shape changes as the spin of the system increases beyond $30\hbar$.

In figure 1b, the proton separation energy S_P as a function of various spin and temperature is shown. Its behavior is slightly different from the one for neutron separation energy at high spins. Although S_P is drastically lowered by about 0.5 to 1.0 MeV, proton emission [29] is inhibited by the Coulomb barrier. Since the nuclei are deformed, the barrier height is not uniform along the nuclear surface. Emission of protons in regions of lower Coulomb barrier height is still possible at high spins.

In figure 1c, the variation of S_N (dashed line) with spin M is shown for $T = 0.3$ MeV, when the pairing correlations are important; S_N fluctuates with spin because of shape fluctuations. For $I > 20\hbar$, the pairing gap $\Delta_n \to 0$, is indicating superfluid to normal state transition since collective rotation tends to break the pairs as spin increases. In figure 1d, the proton separation energy as a function of M is shown for $T = 0.3$ MeV. The trends are the same as that of S_N. At $T > 0.5$ MeV and $I > 10\hbar$, the pairing gap $\Delta_p \to 0$ when the nuclear transitions from superfluid to normal state occur, these fluctuations disappear.

In figures 2a and 2b the corresponding values of the level density parameter are shown as a function of temperature and spin. The single particle level density parameter a for all M values shows a linear behavior for temperature greater than 1.0 MeV. This aspect has been already reported by us in an earlier work on level density parameter [13]. The curve shows a minimum around $I = 55\hbar$ for all the nuclei considered in this text. From shell correction point of view, a lower value of a indicates relatively greater stability of the system. The shape transitions around these angular momentum states are due to the minimization of the energy of the system with respect to shape parameters a_0 and a_2. The rotational energy is lowered by these shape transitions and the angular momentum states beyond these transition points correspond to the different shapes brought about by the minimization of energy. It is also referred to as band crossing as indicated in the insert figures 3a–3d by dotted lines which are extrapolation of the different bands. For ^{155}Er, ^{165}Er, ^{167}Yb and ^{187}Hg, a single band crossing around $I = 55\hbar$ is observed. The total excitation energy E^* of the system corresponding to the temperature 0.8 MeV is 30 MeV. The rotational energy $E_{\rm rot}$ of the residual nucleus is used in the calculation of neutron emission probability.

At the band crossing due to shape changes, the moment of inertia changes sharply and these are shown in figures 4a–4d. The dotted line corresponds to the rigid body moment of inertia of the spherical nucleus. In figures 4a–4d only θ_1 values defined by eq. (5.7) are shown and the line connecting the moments of inertia curve around band crossing indicates that θ_2, defined by eq. (5.8), is the more appropriate definition of the moment of inertia.

The values of the parameter depicted in figures 1–4 are very important in the determination of neutron emission probability at high spins. This is obvious from eq. (5.9). In our earlier work [1] we reported the results for ^{156}Er. The obtained neutron emission probability agreed very well with experimental results of Henss *et al* [2]. There we were also able to explain that it would be very conducive for the study of neutron emission spectra around $I \approx 50\hbar$ and experimental data were indeed for $I \approx 52\hbar$.

In figures 5a–5d neutron emission spectra for various angular momenta are shown for the nuclei ^{156}Er, ^{166}Er, ^{168}Yb [4] and ^{188}Hg. The curves are all normalized to 2000. As the spin of the system increases, there is a general tendency for the peak at $E_n = 1.0$ MeV to rise, resulting in the lowering of probabilities at higher E_n values but for spins 35 to $45\hbar$ the emission probability for larger E_n values are slightly higher when compared to the emission probability for the spin-less system. At higher E_n values for spin $75\hbar$ the emission probability is lower than that of $0\hbar$. This may be due to the increase in the rotational energy of the systems at higher spins and a greater part of the excitation energy is associated with the collective rotation degree of freedom.

Since two methods are available for the study of high spin hot systems as stated in the introduction, we show in figures 6a–12b the values of the different parameters calculated by the two methods for the nucleus ^{186}Hg. In figures 6a and 6b the values of the Lagrangian multiplier γ and collective rotation ω as a function of temperature and spin are shown. In figure 6b the values of the Lagrangian multiplier γ and collective rotation ω as a function of temperature and spin are shown. In figure 6a for $M = 30\hbar$, γ and ω are plotted as a function of T for various deformation parameters. When the deformation parameter $a_2 = 0$, i.e., for biaxial deformation, $\gamma = \omega$ for all values of M and T. However, for $a_2 \neq 0$, $\gamma \neq \omega$, since triaxial deformations mixes states of different spin projections $+m_z$. In figure 6b for $T = 1.0$ MeV, γ and ω are plotted vs. M.

It is obvious from figure 6a that γ is very sensitive to the deformation parameter a_2. For a change of a_2 from 0.0 to 0.03, γ changes from 0.35 to 0.4 MeV whereas the corresponding changes in ω values are smaller.

In figures 7a and 7b, for ^{186}Hg, the collective rotational frequency ω and γ are plotted vs. M for temperature 0.3 MeV and 1.0 MeV. For prolate deformation the CNM calculation shows a shape transition beyond $\omega = 0.3$ MeV whereas the STHR calculation shows shape transition around $\gamma = 0.15$ MeV in addition to the one at 0.3 MeV. At $T = 1.0$ MeV, in the STHR, this shape transition at small frequencies still exists but the ones at higher frequencies vanish in both the methods. In the case of oblate deformation both the methods yield almost the same results at high temperatures.

In figures 8a and 8b, the corresponding rotational energies are shown as a function of collective rotational frequency. In view of figures 7a and 7b the results shown in figures 8a and 8b are self explanatory. The fluctuation at $\omega = 0.15$ MeV corresponding to an angular momentum of $5\hbar$ in the case of prolate deformations, is similar to the one observed in experiments as back bending phenomena [15].

The fluctuation at $5\hbar$ observed in figures 8a and 8b is also exhibited in figures 9a and 9b which shows the single particle level density parameter a as a function of M for $T = 1.0$ MeV. In figures 10a, 10b, 11a and 11b the neutron and proton separation energies obtained from the two methods are shown.

In figures 12a and 12b the variation of the gap parameter Δ_n and Δ_p for $T = 0.3$ MeV, obtained by solving eqs (3.2), (3.3) and (3.5) in the STHR and the set of eqs (4.2), (4.3) and (4.5) in the CNM, for ^{186}Hg are displayed. In figure 12a, curves 1 and 2 represent the Δ_n values obtained in the STHR and CNM calculations respectively, for deformation parameter values $a_0 = 0.6$ and $a_2 = 0.06$. The values of γ and ω are shown along x-axis. Clearly the structure exhibited in the CNM calculation is absent in the STHR calculation. The former is a more microscopic calculation due to the inclusion of the coupling between the collective rotation and the single particle spins in the Hamiltonian itself. Since triaxial deformations couple states of different m_z, the rotational part of the Hamiltonian is affected. The nuclear structural effect on Δ_n and Δ_p are more pronounced in the CNM calculation. The spins generated are also presented in the same figures (curves 3 and 4) for direct comparison.

7. Conclusion

In conclusion we state that neutron and proton separation energies are very sensitive to the structural transitions in high spin hot nuclear systems. Its role in the determination of single neutron emission in high spin nuclei is very well brought out in the present analysis. However, the effect of surface diffuseness on neutron separation energy has not been studied in the present work. Finally by extending the microscopic cranked Nilsson model to hot nuclei we were able to show that certain features of the structural transitions in ^{186}Hg is explained very well by the CNM calculation rather than by the STHR.

Acknowledgements

This work is dedicated to the memory of (late) Dr M R Rajasekeran, Department of Nuclear Physics, University of Madras, Chennai. Useful discussion with Prof V Devanathan is gratefully acknowledged. SS would like to thank University Grants commission, India,

for providing leave under Faculty Improvement Programme. The partial support by FIST, Department of Science and Technology, India is also gratefully acknowledged.

References

[1] M Rajasekaran, T R Rajasekaran, N Arunachalam and V Devanathan, *Phys. Rev. Lett.* **61**, 2077 (1988)
[2] S Henss, A Ruckelshausen, R D Fisher, W Kuhn, V Metag, R Novotny, R V F Janssens, T L Khoo, D Habs, D Schwalm, D Freeman, G Duchene, B Hass, F Hass, S Hlavac and R S Simon, *Phys. Rev. Lett.* **60**, 11 (1988)
[3] A S IIjininov *et al*, *Nucl. Phys.* **A543**, 517 (1992)
[4] R J Charity *et al*, *Phys. Rev.* **C63**, 024611 (2001)
[5] L G Moretto, *Nucl. Phys.* **Al82**, 641 (1972); **Al85**, 145 (1972); **A216**, 1 (1973)
[6] J B Huizenga and L G Moretto, *Annu, Rev. Nucl. Sci.* **22**, 427 (1972)
[7] D R Inglis, *Phys. Rev.* **96**, 1059 (1954)
[8] I Hammamotto, *Treatise on heavy-ion science, compound system phenomena* edited by D A Bromley (Plenum, New York, 1985) vol. 3, p. 313
[9] G Shanmugam, P R Subramanian, M Rajasekaran and V Devanathan, Nuclear Interactions, *Lecture Notes in Physics* edited by B A Robson (Springer, Berlin, 1979) vol. 92, p. 433
[10] J M Eisenberg and W Greiner, *Nuclear models* (North-Holland, New York, 1975) p. 451
[11] M Rajasekaran and V Devanathan, *Phys. Lett.* **B104**, 95 (1981); **B113**, 433 (1982); *Phys. Rev.* **C24**, 2606 (1981)
[12] M Rajasekaran, N Arunachalam and V Devanathan, *Phys. Rev.* **C36**, 1860 (1987)
[13] M Rajasekaran, T R Rajasekaran and N Arunachalam, *Phys. Rev.* **C37**, 307 (1988)
[14] M Rajasekaran, N Arunachalam, T R Rajasekaran and V Devanathan, *Phys. Rev.* **C38**, 1926 (1988)
[15] F Hannachi, G Bastin, M G Porguet, C Schuck, J P Thibaud, C Bourgeois, L Hildingsson, D Jerrestam, N Perrin, H Sergolle, F A Beck, T Byrski, J C Merdinger and J Dudek, *Nucl. Phys.* **A481**, 313 (1985)
[16] J Sauvage *et al*, *Acta Physica Polanica* **B30**, 1393 (1999)
[17] H T Duong *et al*, *Phys. Lett.* **B217**, 401 (1989)
[18] T Hiberath *et al*, *Z. Phys.* **A342**, 1 (1992)
[19] B Roussiere *et al*, *Nucl. Phys.* **A504**, 511 (1989)
[20] G Shanmugam and V Devanathan, *Phys. Scr.* **24**, 17 (1981); **25**, 607 (1982)
[21] T Bengtsson, *Nucl. Phys.* **A496**, 56 (1989); **A512**, 124 (1990)
[22] V G Soloviev, *Theory of complex nuclei* (Pergamon, Oxford, 1976) p. 20
J M Eisenberg and W Greiner, *Microscopic theory of the nucleus* (North-Holland, New York, 1976) p. 399
[23] I Hammamotto, *Phys. Scr.* **T5**, 10 (1983)
[24] J M Blatt and V F Weisskopf, *Theoretical nuclear physics* (Springer, New York, 1979)
[25] K Snover, *Annu. Rev. Part. Nucl. Sci.* **36**, 545 (1986)
[26] R J Charity, *Phys. Rev.* **C64**, 064610 (2001)
[27] N Nica *et al*, *Phys. Rev.* **C64**, 034313 (2001)
[28] H W Cranmer-Gorden, P D Forysth, D V Elenkov, D Howe, J P Sharpey-Schafer, M A Riely, G Selton, J Simpson, I Ragnarsson, Z Xing and T Bengstsson, *Nucl. Phys.* **A465**, 506 (1987)
[29] Z He, J Wu and W Norenberg, *Nucl. Phys.* **A489**, 421 (1988)